

Contents lists available at [SciVerse ScienceDirect](http://www.sciencedirect.com)

# Earth and Planetary Science Letters

journal homepage: [www.elsevier.com/locate/epsl](http://www.elsevier.com/locate/epsl)

## Olivine rheology, shear stress, and grain growth in the lithospheric mantle: Geological constraints from the Kaapvaal craton

Xu Chu\*, Jun Korenaga

Department of Geology and Geophysics, Yale University, New Haven, CT 06520, USA

### ARTICLE INFO

#### Article history:

Received 16 October 2011

Received in revised form

28 February 2012

Accepted 13 April 2012

Editor: Y. Ricard

#### Keywords:

Mantle rheology

lithospheric stress

grain-growth laws

### ABSTRACT

The rheology of Earth's mantle is a complex function that depends on, at least, temperature, pressure, stress, grain size, and water content. Understanding this functionality is of fundamental importance in mantle dynamics, but constraints from laboratory experiments entail considerable extrapolation. Here we propose a new observational approach based on a unique tectonic setting of the Kaapvaal craton, which allows us to exploit its continental lithosphere as a natural laboratory. Mantle xenoliths brought to the surface by kimberlites in the Kaapvaal craton delineate a representative thermal profile, and the spatial distribution of their ages provides a tight constraint on a lithospheric-scale deformation history. Combined with a simple modeling of the thermal and dynamic evolution of the upper mantle subject to continental drift, these xenolith-based observations can test the validity of existing flow laws at geological strain rates, estimate the magnitude of shear stress in the upper mantle, and constrain the effective grain-growth rate at lithospheric conditions. Calculated displacements relative to surface over the last 3.5 billion years, with flow-law parameters recommended by [Korenaga and Karato \(2008\)](#), are found to be consistent with geochronological observations. Our results also indicate that shear stress has been increasing in the past 3.5 billion years, owing to the cooling of the ambient mantle, within the range of 0.01–0.1 MPa. Though this range of shear stress is about two orders of magnitude lower than that predicted by grain-size-based piezometers, greater stress would lead to too large displacement across the lithosphere to be consistent with its geochronological pattern. The grain size of olivine in mantle xenoliths is typically 5–10 mm, which is too small to be at a dynamical equilibrium with the estimated stress, suggesting that grain growth is considerably suppressed by some mechanism such as orthopyroxene pinning.

© 2012 Elsevier B.V. All rights reserved.

### 1. Introduction

The Kaapvaal craton covers an area of  $1.2 \times 10^6$  km<sup>2</sup> in southern Africa, bounded by the Archean Limpopo belt to the north and the Proterozoic mobile belts to the south and west ([Fig. 1a](#)). This cratonic lithosphere provides a direct record of pristine Archean lithosphere, with the age of the oldest exposed rock being 3640 Ma ([de Wit et al., 1992](#)), and has been stabilized for at least the last 2.9 Gyr since the collision between the eastern Witwatersrand and western Kimberley blocks ([Schmitz et al., 2004](#)). The thick and stable craton was subsequently intruded by kimberlites of the Cretaceous or older ages, and mantle xenoliths brought up by kimberlite magmatism provide a lithospheric profile at the time of eruption. In this study, we combine major features of these xenoliths with a simple model of lithospheric evolution to infer the dynamic state of the subcontinental lithospheric mantle.

By doing so, we are also able to test existing flow laws for mantle rheology and to place some constraints on grain-growth kinetics under lithospheric conditions.

Our knowledge of the rheological behaviors of Earth's mantle has been steadily increasing, owing to progress made in rock deformation experiments, geodetic observations, and geological studies of exhumed mantle rocks in shear zones (e.g. [Bürgmann and Dresen, 2008](#)). Typical peridotites from subcontinental lithospheric mantle consist of more than 70% volume fraction of olivine, so olivine is commonly regarded as the governing phase for the rheology of the upper mantle. Two major mechanisms of plastic deformation in olivine are dislocation creep and diffusion creep, and both mechanisms are known to be affected by the presence of water ([Mei and Kohlstedt, 2000a, b](#)). Each mechanism of plastic deformation can be described in the following form:

$$\dot{\epsilon} = Ad^{-m} \sigma^n C_{OH}^r \exp\left(-\frac{E+pV}{RT}\right), \quad (1)$$

where  $\dot{\epsilon}$  is strain rate,  $A$  is a pre-exponential factor,  $d$  is grain size,  $m$  is grain-size exponent,  $\sigma$  is deviatoric stress,  $n$  is stress

\* Corresponding author.

E-mail address: [xu.chu@yale.edu](mailto:xu.chu@yale.edu) (X. Chu).

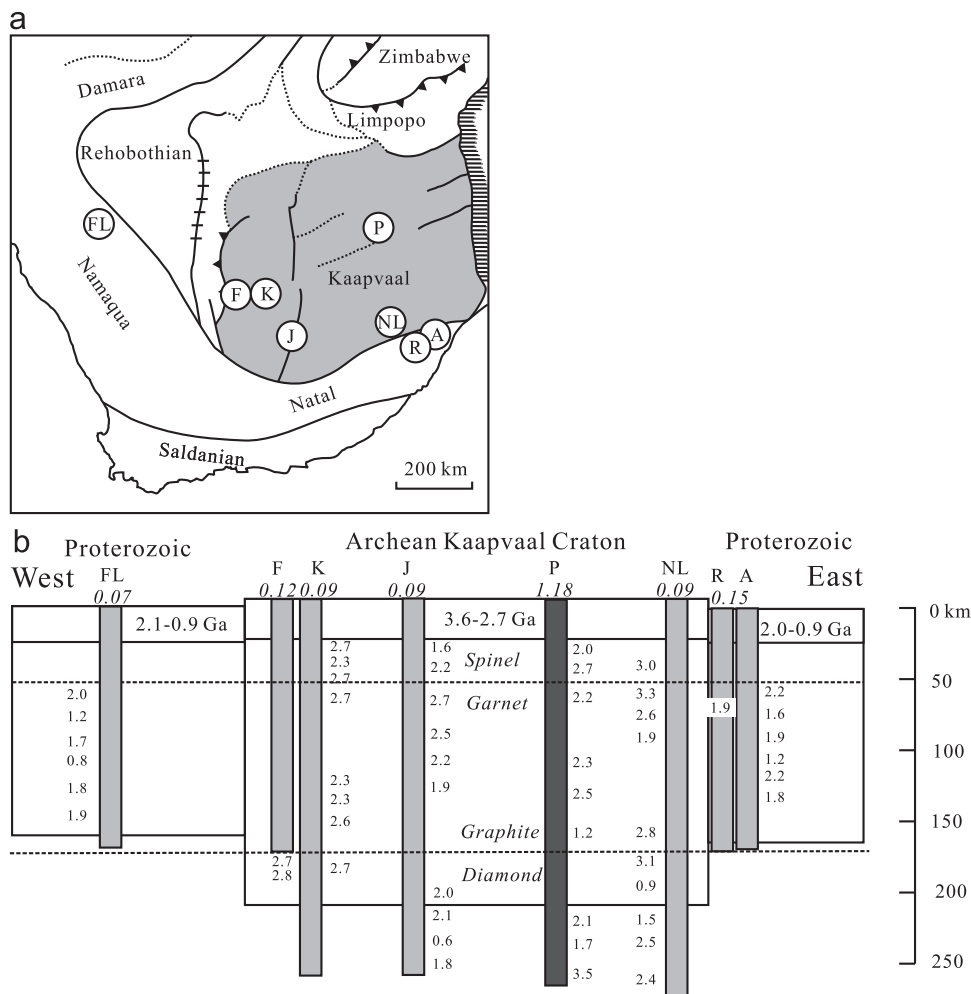


**Fig. 1.** (a) Schematic geologic map showing major structural units in southern Africa, with Kaapvaal Craton in shaded area (after Griffin et al. (2003)). Also shown are the present locations of kimberlite fields sampled by Pearson (1999) (b). Abbreviation of kimberlite fields: FL—Farm Louwrencia; J—Jagersfontein; F—Finsch; K—Kimberley; P—Premier; NL—North Lesotho; R—Ramatselisio; A—Abbotsford. (b) Schematic cross-section of southern Africa showing Re-depletion model ages (in Ga) at depths corresponding to selected xenoliths from individual kimberlite pipes (after Pearson (1999)). Labels on the top of kimberlite pipes correspond to the locations in Fig. 1a. Also shown on the top in italic are the kimberlite ages.

exponent,  $C_{OH}$  is water content (usually in ppm H/Si),  $r$  is water exponent,  $E$  is activation energy,  $p$  is pressure,  $V$  is activation volume,  $R$  is the universal gas constant, and  $T$  is absolute temperature. Different deformation mechanisms correspond to different sets of flow-law parameters ( $A$ ,  $m$ ,  $n$ ,  $r$ ,  $E$ , and  $V$ ), and even in the same type of creep mechanism (i.e., diffusion or dislocation), flow-law parameters are different under water-saturated ('wet') and water-unsaturated ('dry') conditions. The grain-size exponent  $m$  is zero for dislocation creep, the stress exponent  $n$  is unity for diffusion creep, and obviously, the water exponent  $r$  is zero for deformation under 'dry' conditions. The number of nontrivial flow-law parameters for diffusion and dislocation creep under 'dry' and 'wet' conditions is therefore 18 (four  $A$ 's, two  $m$ 's, two  $n$ 's, two  $r$ 's, four  $E$ 's, and four  $V$ 's).

These flow-law parameters have to be determined by laboratory experiments on rock deformation, but such experiments suffer from several intrinsic drawbacks. Strain rates that can be achieved in laboratory are usually of the order of  $10^{-5} \text{ s}^{-1}$ , many orders of magnitude higher than geological strain rates ( $10^{-14}$ – $10^{-15} \text{ s}^{-1}$ ); such high strain rate is necessary to produce observable deformation within a timescale of hours or days. The limited temperature and pressure ranges explored in experiments also result in uncertain extrapolation to higher pressures and temperatures; this problem is especially severe for the pressure

dependence of creep. Given the essential role played by olivine flow laws in mantle dynamics, it is important to test experimentally-derived parameters with geological observations. Previous studies on such geological tests were done in high-strain shear zones, such as exposed mantle peridotite massifs (Vissers et al., 1995; Dijkstra et al., 2004) and subcontinental xenoliths (Gueguen and Nicolas, 1980). These mantle rocks are mylonitized, with significant grain size reduction, so diffusion creep plays a dominant role (Jin et al., 1998; Dijkstra et al., 2004). In this study, we focus on the deformation of continental lithosphere associated with its lateral movements, in which strain rate is much lower than that in a ductile shearing zone.

## 2. Problem setting

The Kaapvaal craton presents a unique opportunity to investigate the thermal and dynamic structure of continental lithosphere over geological time, because kimberlite pipes are both spatially and temporally widespread. Kimberlite pipes sample the lithosphere at different depths, and based on xenoliths from each pipe, we can reconstruct a lithospheric profile at the time of kimberlite eruption. Pearson (1999) applied the Re–Os isotope system to date mantle xenoliths in Kaapvaal kimberlites (Fig. 1b).

The observed Re depletion model age pattern may be summarized as follows. First, the ages are nearly consistent for xenoliths from the same kimberlite pipe, especially for those low-temperature series above 200 km. Second, the ages of xenoliths vary laterally among pipes across the craton. Xenoliths in the North Llesoto pipe have ages of around 3 Ga, while those in other pipes that intruded the Archean Kaapvaal Craton have ages around the Archean–Proterozoic boundary (2.5 Ga). Xenoliths exhumed in Proterozoic terranes have ages of about 2 Ga or younger. Finally, the ages of kimberlites are considerably younger than those of xenolith. Except Proterozoic Finsch pipe, all the other kimberlites are of Cretaceous ages (Fig. 1b). On the basis of this geochronological pattern, Pearson (1999) proposed the 'lateral block accretion' model: blocks were laterally added to a preexisting Archean continental core, and Proterozoic blocks were subsequently accreted to the margins of the Archean craton.

Once we realize that, after fully stabilized around 3 Ga, the Kaapvaal continental lithosphere must have experienced shear deformation associated with continental drift, the above geological observation can be turned into an important constraint on the rheology of lithospheric mantle. That is, the lithospheric mantle beneath the Kaapvaal craton has to be strong enough to preserve the geochronological pattern exhibited by mantle xenoliths over the time scale of billions of years. To this end, we first estimate a likely thermal evolution of the continental lithosphere, and then explore its possible deformation history with a range of olivine flow-law parameters.

We use a simple one-dimensional (1-D) model with constant thickness over time to represent the continental lithosphere. Estimates on the thickness of the continental lithosphere beneath the Kaapvaal craton vary substantially (e.g. James et al., 2001; Eaton et al., 2009; Evans et al., 2011), but diamondiferous xenoliths indicate that the lithosphere is at least 170 km thick. Given that the deepest xenoliths sampled by Pearson (1999) originate at about 250 km, we set 250 km as the base of lithosphere in our model, the choice also adopted by previous studies on the thermal structure of the Kaapvaal lithosphere (McKenzie et al., 2005; Michaut et al., 2007). Seismic surveys show that the average crustal thickness of the Kaapvaal craton is around 35–40 km (Nguuri et al., 2001; Stankiewicz et al., 2002; Niu and James, 2002). Granitic upper crust with higher radiogenic heat production rate is distinguished from mafic lower crust for an accurate calculation of thermal evolution. The base of highly radioactive upper crust, according to geological field studies, is located at the depth of 13 km (Nicolaysen et al., 1981; Jones, 1988).

### 3. Thermal evolution of continental lithosphere

A temperature profile in the lithosphere is calculated by solving 1-D heat conduction (Turcotte and Schubert, 2002) with temperature boundary conditions. The surface temperature is fixed at 25 °C, while the bottom temperature at 250 km depth is time-dependent and calculated from a given potential temperature (a hypothetical temperature of a mantle brought up adiabatically to the surface without melting) with an adiabatic gradient of 0.5 °C/km. For the temporal variation of mantle potential temperature, we use the prediction from the thermal evolution model of Korenaga (2006, 2008), which has been shown to be consistent with petrological constraints on the secular cooling of the upper mantle (Herzberg et al., 2010). An alternative boundary condition in previous studies (Jaupart and Mareschal, 1999; McKenzie et al., 2005; Michaut et al., 2007) is related to the basal heat flux sustained by underlying convecting mantle. Whereas solving heat conduction with the heat flux boundary condition is equally straightforward, the temporal evolution of the basal heat

flux is poorly known, so this type of boundary condition is not considered in this study. This temperature boundary condition results in a discontinuity in heat flux at the boundary, but in reality, such discontinuity would be quickly smoothed by the growth of a thermal boundary layer beneath the lithosphere. Due to convective instability, the thermal boundary layer would repeatedly experience growth and destruction (e.g. Korenaga and Jordan, 2002), and our choice of the bottom boundary condition aims to capture the first-order influence of asthenospheric "heat bath" on continental lithosphere, without dealing with the dynamics of such small-scale convection.

Thermal conductivities and their temperature dependency are adopted from Chapman and Furlong (1992), Hofmeister (1999) and Whittington et al. (2009). The temperature-dependent heat capacities and densities for different layers of lithosphere are calculated with an internally-consistent thermodynamic dataset for minerals (Holland and Powell, 1998), together with the proportions of major phases. Internal heating within the lithosphere is caused by the decay of four radioactive isotopes:  $^{235}\text{U}$ ,  $^{238}\text{U}$ ,  $^{232}\text{Th}$ , and  $^{40}\text{K}$ . Their half-lives and rates of heat generation are summarized in Turcotte and Schubert (2002). The concentrations of these isotopes in the continental lithosphere are from Taylor et al. (1981) and further adjusted by field observations and measurements, as summarized in Michaut et al. (2007). The details of model parameters are given in Appendix A.

We use a forward-time-central-space finite difference method (Press et al., 1992) with a time step of 10 Myr and a depth interval of 1 km. We do not assume a steady state *a priori* to take into account the effect of transient cooling. The initial conditions are largely unknown, so we start with random initial conditions at 4 Ga (Fig. 2). Initial geotherms are randomly chosen within two adiabatic geotherms with the surface temperatures of  $T=25\text{ °C}$  and  $T=T_p$ . Calculated temperature profiles converge after one billion years, as expected from the thermal diffusion time scale. The diffusion time scale is given by  $L^2/\kappa$  (e.g. Turcotte and Schubert, 2002), where  $L$  is a length scale (250 km) and  $\kappa$  is the thermal diffusivity (about  $1 \times 10^{-6}\text{ m}^2/\text{s}$ ), and is about two billion years in this case. A steady state is typically achieved within a fraction of the diffusion time scale. The calculated temperature profiles agree well with the geothermobarometry of mantle xenoliths, which has been extensively studied for the Kaapvaal craton (Fig. 3). In the subsequent section, we ignore the first 0.5 Gyr of the calculated thermal history, which is highly variable because of random initial conditions, and focus on thermal evolution from 3.5 Ga to present. We further compare the 1000 calculated thermal profiles with thermobarometry results derived from mantle xenoliths (e.g. Boyd and Nixon, 1975; Danchin, 1979; Lazarov et al., 2009) and choose the one that matches xenolith data most closely as the best-fit profile for the following calculations (Fig. 3).

### 4. Dynamic evolution of subcontinental lithospheric mantle

#### 4.1. Model formulation and flow-law parameters

We assume that a relatively depleted 'dry' lithospheric mantle overlies a 'wet' convective upper mantle (Fig. 4). The bottom boundary at 410 km is set to be non-slip, i.e., zero horizontal velocity at the bottom. If flow in the transition zone shares the same direction with that in the upper mantle, this non-slip boundary condition overpredicts shear stress and strain rate, but the opposite case could have also occurred during the last few billion years. The non-slip boundary condition is thus chosen as a neutral choice. With this bottom boundary condition, the surface velocity  $v_{plate}$ , is simply a depth integral of strain rate

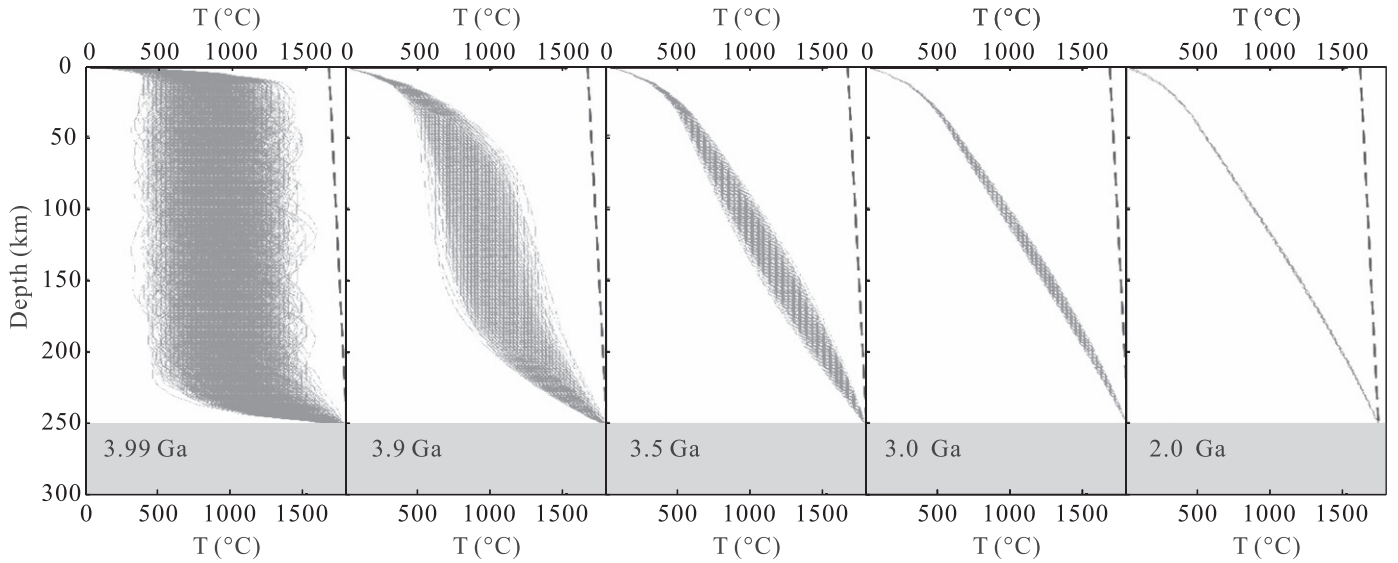


**Fig. 2.** 1000 temperature profiles calculated with random initial conditions at 4.0 Ga and temperature boundary conditions (see text for details). Discrepancies due to random initial conditions diminish mostly after the first 1 billion years.

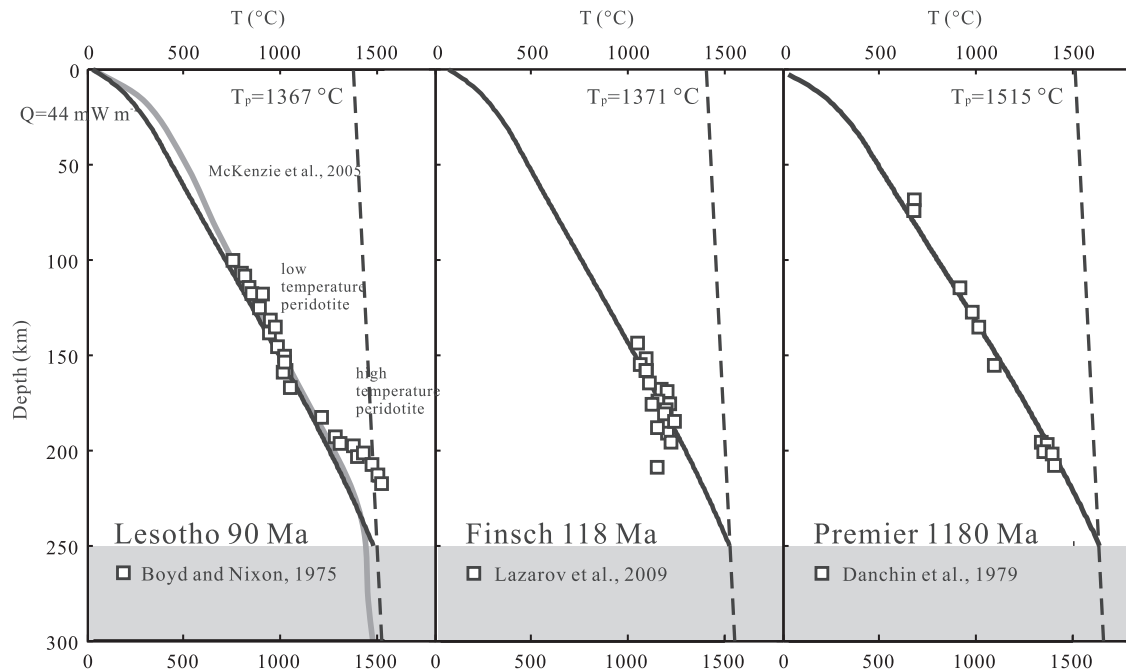


**Fig. 3.** Thermal structure of Kaapvaal cratonic lithosphere based on our modeling results (solid curve) that best fit the estimated P–T conditions of mantle xenoliths (squares; Lesotho, Boyd and Nixon, 1975; Finsch, Lazarov et al., 2009; Premier, Danchin, 1979). Present-day thermal profile calculated by McKenzie et al. (2005) is also shown for comparison (gray curve).

through the upper mantle:

$$v_{plate}(t) = \int_{410 \text{ km}}^{0 \text{ km}} \dot{\epsilon}(t, z) dz. \quad (2)$$

As shown in Eq. (1), the strain rate depends on flow-law parameters as well as environmental variables. We adopt the set of olivine flow-law parameters recommended by Korenaga and Karato (2008) (Appendix B), in which a number of rock deformation data are integrated in a consistent statistical framework. For the environmental variables, we use best-fit temperature profiles obtained in the previous section (Fig. 3) and calculate corresponding pressure profiles using the equations of state for mantle rocks. A temperature profile through the convective mantle is an adiabatic thermal profile that continues from the basal temperature of

the lithosphere. For the sake of simplicity, ductile deformation in a cold and stiff crustal layer is assumed to be insignificant.

Because diffusion creep and dislocation creep can occur in parallel, the total deformation is a sum of contributions from both mechanisms:

$$\dot{\epsilon} = \dot{\epsilon}_{diff} + \dot{\epsilon}_{dis}. \quad (3)$$

For each mechanism, a flow law depends on the water content of olivine, and after calculating strain rates with both ‘dry’ and ‘wet’ flow laws, a greater strain rate is considered to be what actually takes place, i.e.,

$$\dot{\epsilon} = \max(\dot{\epsilon}_{wet}, \dot{\epsilon}_{dry}). \quad (4)$$

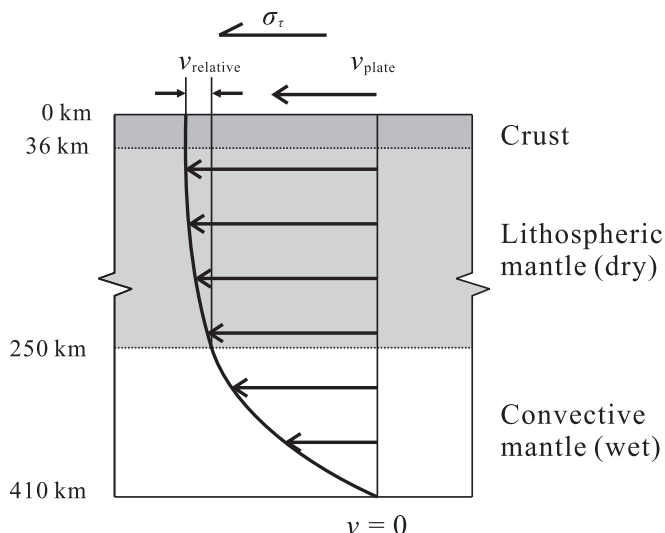


**Fig. 4.** Cartoon illustrating our flow model composed of 250 km-thick lithosphere and underlying convective upper mantle. With no variation in the horizontal direction, momentum balance dictates that shear stress is constant throughout the section. The basal boundary at 410 km is assumed to be non-slip. Difference in strain rate between the top and bottom of lithosphere leads to relative displacement within lithosphere.

With a very low water content, for example, a ‘wet’ flow law predicts a diminishingly small strain rate, and in this case, a ‘dry’ flow law provides a realistic estimate on strain rate. Measurements of water content as high as  $\sim 800$  ppm H/Si have been reported for mantle xenoliths (Miller et al., 1987; Bell and Rossman, 1992; Kurosawa et al., 1997), which are even higher than for the wedge mantle in subduction zone (Peslier and Luhr, 2006). This high water content, however, contradicts deformation microstructures observed in olivine (Katayama and Korenaga, 2011). A recent study by Peslier et al. (2010) suggests that the water content is about 85 ppm  $\text{H}_2\text{O}$  (233 ppm H/Si) at the maximum and is probably about 60 ppm  $\text{H}_2\text{O}$  (164 ppm H/Si) on average. Their study also indicates that the water content is nearly constant with pressure less than 5 GPa (above 155 km depth) and decreases to around zero at 7 GPa ( $\sim 220$  km depth). However, the number of samples from greater than 5 GPa is limited, so we set the water content of the lithospheric mantle uniformly to 164 ppm H/Si. The water content of the underlying convective mantle is set to 800 ppm H/Si (Hirth and Kohlstedt, 1996).

The grain size of olivine is assumed to be 7 mm, based on measurements in mantle xenoliths collected from the Kaapvaal craton (e.g. Ave Lallement et al., 1980). This leaves the deviatoric shear stress as the only unknown in the flow-law equation (Eq. (1)). For this Couette-flow-type model (Fig. 4), shear stress is constant across the whole layer, and for a given surface velocity, Eq. (2) can be solved numerically for such constant shear stress. Even if surface velocity does not change with time, shear stress still varies with time because the time-dependent temperature profile affects mantle rheology. Present-day surface velocity at southern Africa is about 7 mm/yr in the hotspot reference frame (Gripp and Gordon, 2002). The variation of plate velocity in the past can be obtained from paleogeomagnetic studies (e.g., Jurdy et al., 2005) and can also be estimated based on the thermal evolution of Earth (Korenaga, 2006, 2008). We will test several possibilities on the temporal variation of plate velocity.

As the thermal structure of the lithosphere becomes more uncertain at greater ages (Fig. 2), the time integration of strain rate is conducted backward in time, starting at the present day. Relative displacement with respect to the surface is calculated as

a function of time, for different depths in the lithosphere. The kimberlite pipes studied by Pearson (1999) are separated from each other by about a hundred kilometers, so the lateral displacement across the lithosphere must be on the same scale at most; otherwise the geochronological pattern in mantle xenoliths would be severely destroyed.

#### 4.2. Model results

Modeling results for shear stress and relative displacement are presented in Fig. 5 for a variety of cases (see also Appendix C). As one of the common features among all cases considered, shear stress in the upper mantle has been gradually increasing for the last 3 Gyr, because the mantle is cooling and becoming more viscous. The magnitude of stress is in the range of 0.01–0.06 MPa, about two orders of magnitude lower than the stress previously obtained with grain-size-related piezometers (e.g., 4–6 MPa; Ave Lallement et al., 1980). For the reference case shown in Fig. 5a (the case with 164 ppm H/Si), relative displacements over the last 3.5 Gyr are 15 km, 58 km and 190 km, respectively, at the depths of 200 km, 225 km, and 250 km. Relative displacements at depths shallower than 200 km are therefore small enough to preserve the geochronological pattern described by Pearson (1999). The displacement at the depth of 250 km is large, but xenoliths from around this depth belong to the ‘sheared’ or ‘high temperature’ series (Boyd and Nixon, 1975; Pearson et al., 1995; Pearson, 1999).

To test the robustness of the reference case, we perturb it for the water content of the lithospheric mantle, the water content of the convective mantle, grain size, and plate velocity. Shear stress is almost independent of the water content of the lithosphere (Fig. 5a) although weaker lithosphere due to higher water content leads to a slightly greater displacement (Fig. 5b). This weak sensitivity is understandable because most of the shearing takes place in the weak convective mantle, but non-zero sensitivity also indicates that the flow-law parameters for the ‘wet’ condition are what controls lithospheric deformation. When the convective mantle is dryer and more viscous, higher shear stress is required to maintain the same plate velocity (Fig. 5c), and higher stress results in greater displacement in the lithosphere (Fig. 5d). Results with different grain sizes show that, near the base of the lithosphere, strain rate due to diffusion creep is comparable to but smaller than that due to dislocation creep (Fig. 5f; compare the cases with grain size of 7 mm and with infinite grain size at 250 km, the latter having no contribution from diffusion creep), while in shallower lithospheric mantle, diffusion creep overweighs dislocation creep. Nevertheless, integrated displacement is mostly due to deformation at the bottom of lithosphere, so the effect by neglecting diffusion creep is trivial. In the convective mantle where temperature increases only adiabatically but pressure increases linearly with depth, dislocation creep, which has a smaller activation volume than diffusion creep, dominates ductile deformation. As a result, shear stress is virtually insensitive to changes in grain size, even when varied from 2 mm (close to coarse mylonitic peridotite) to infinity (Fig. 5e). Too small a grain size does, however, lead to a geologically unacceptable situation; in the case of grain size of 2 mm, relative displacements within much weakened lithosphere dramatically increase to thousands of kilometers (Fig. 5f). Finally, higher plate velocity leads to higher shear stress (Fig. 5g) and greater displacement (Fig. 5h).

The reference model calculation is repeated with flow-law parameters recommended by Hirth and Kohlstedt (2003). At 200 km depth displacement over the past 3.5 Gyr is 116 km, which is one order of magnitude larger, but still lies in reasonable bounds. Shear stress at present is accordingly similar to the result with the parameters of Korenaga and Karato (2008), but the shear

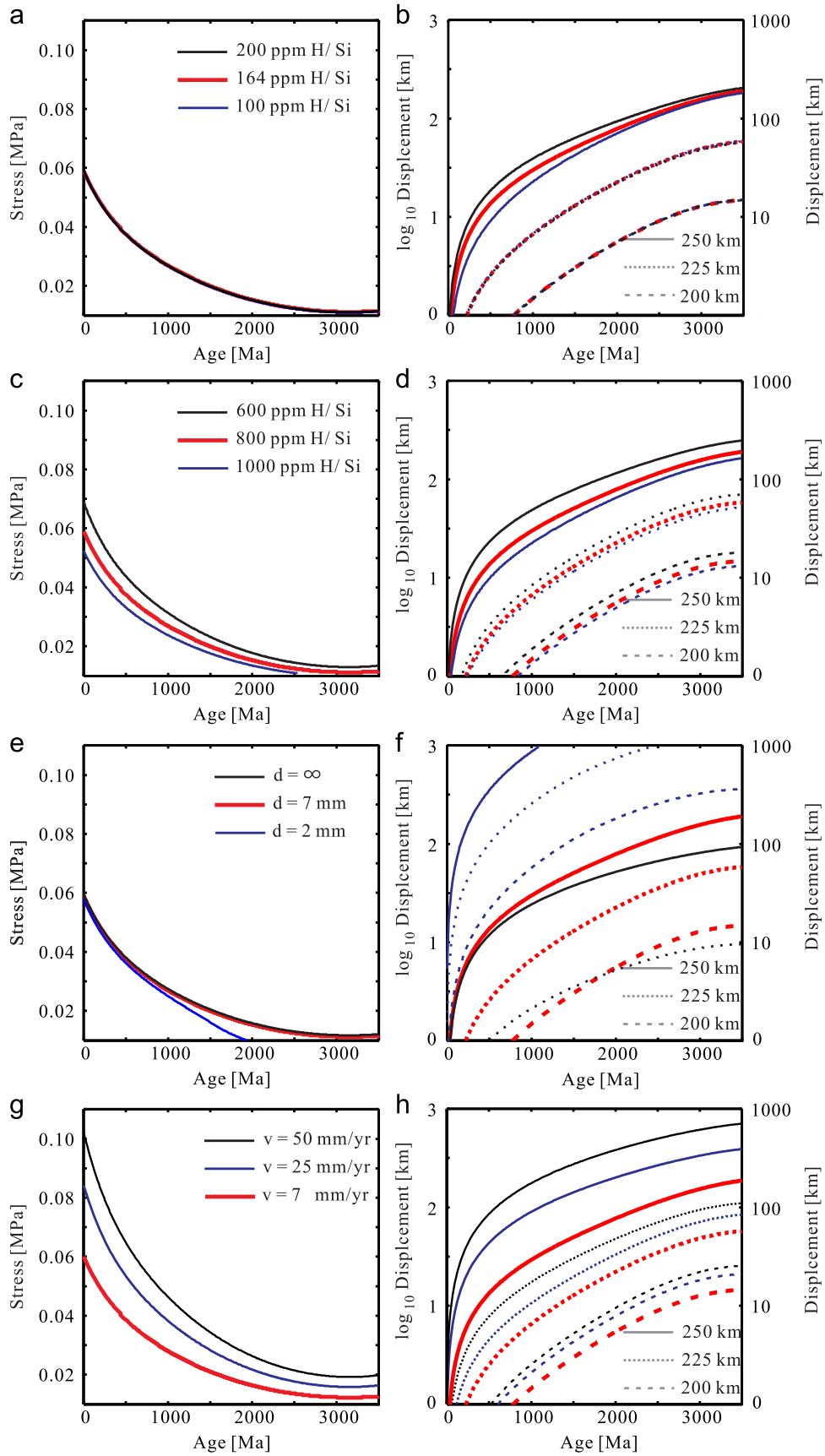


**Fig. 5.** Results of dynamic modeling in terms of stress evolution (left) and surface displacement with respect to certain depths (200 km, 225 km and 250 km) measured from the present (right). Thick red curves denote results with standard conditions (grain size of 7 mm, plate velocity of 7 mm/yr, and water contents of 164 ppm H/Si in lithosphere and 800 ppm H/Si in convective mantle; see text for details). Black and blue curves denote modeling results from sensitivity analysis: (a, b) varying water content in lithospheric mantle; (c, d) varying water content in convective mantle; (e, f) varying grain size; and (g, h) varying plate velocity. (For interpretation of the references to color in this figure legend, the reader is referred to the web version of this article.)

stress evolution curves are more concave. Sensitivity analysis shows that the parameters of Hirth and Kohlstedt (2003) lead to the greater sensitivity of predicted stress to grain size and plate velocity.

We also consider the effect of time-dependent plate motion (Fig. 6). One example is the history of plate velocity predicted from the thermal evolution model of Korenaga (2006). Hotter mantle in the past results in a higher degree of partial melting and leaves more depleted and viscous residue, making mantle convection more sluggish. This plate velocity prediction is regarded as a global average, normalized with the present-day value of 40 mm/yr, and is consistent with the supercontinental cycle (Hoffman, 1997) and with the life span of passive margins (Bradley, 2008). Moreover, for plate motion in the Phanerozoic, a more refined model specific to the African continent based on paleogeomagnetic reconstruction (Jurdy et al., 1995) can be adopted, but these subtle features in plate velocity evolution neither lead to significant change in the general trend of stress evolution (Fig. 6b) nor relative displacements in the lithosphere (Fig. 6c).

To summarize, our results indicate that, in the lithospheric mantle, viscous deformation is controlled by 'wet' creep mechanisms, and strain rate by diffusion creep is comparable to dislocation creep, or even larger at shallower depths, whereas estimated shear stress is controlled mostly by dislocation creep in the convective mantle. Relative displacements across the lithosphere predicted with the flow-law parameters of Korenaga and Karato (2008) are consistent with major geological constraints from mantle xenoliths. We are thus reasonably confident with our estimates on the magnitude of shear stress in the upper mantle and its secular evolution.

## 5. Discussion

### 5.1. Sensitivity to olivine flow-law uncertainty

We used the set of flow-law parameters recommended by Korenaga and Karato (2008), who constructed a comprehensive statistical framework to analyze different deformation data in a coherent manner and estimate full parameter uncertainty including covariance. Each flow-law parameter comes with its own uncertainty, but it is important to realize that one cannot vary one parameter independently with others. For example, they estimated the activation volume for 'wet' dislocation creep to be  $4 \pm 3 \text{ cm}^3/\text{mol}$ , but if one wishes to see the consequence of using

its low-end value (i.e.,  $1 \text{ cm}^3/\text{mol}$ ), the pre-exponential factor  $A$  in Eq. (1) must be adjusted properly following their statistical framework. Otherwise, a resulting flow law would become inconsistent with existing rock deformation data. While one may intuitively expect lower viscosity and thus greater displacement for lower activation volume, the pre-exponential factor decreases at the same time, and this decrease more than compensates for the decrease in activation volume, resulting in higher viscosity and smaller displacement. Thus, a good understanding of the statistical framework developed by Korenaga and Karato (2008) is essential when investigating the effect of flow-law uncertainty. As discussed in the previous section, 'wet' dislocation creep dominates ductile deformation in the upper mantle, so we focus on this deformation mechanism.

Fig. 7 illustrates the dependence of relative displacement at the depth of 200 km on flow-law parameters. The results indicate that large activation energy and small activation volume favor small displacement. At the recommended bounds of activation energy (423–623 kJ/mol) and activation volume ( $1\text{--}7 \times 10^{-6} \text{ m}^3/\text{mol}$ ), the displacement minimum is as low as 7 km, while the largest displacement is 64 km, reached at largest activation volume and smallest activation energy, still lies in an acceptable range (i.e., less than 100 km) (Fig. 7a). At the same depth with the same setting, displacement calculated with the parameters of Hirth and Kohlstedt (2003) nearly doubles the maximum in the above bounds. We also calculate the dependence of displacement on the activation energy and activation volume of 'wet' diffusion creep, but the difference between the maximum and minimum is only about 0.2 km at 200 km depth, with varying these parameters in their recommended ranges.

The uncertainty of the water exponent does not significantly affect displacement (Fig. 7b), which is understandable in this problem setting; when the water exponent varies, the viscosities of the lithospheric mantle and the convective mantle change nearly proportionally, so the proportion of displacement experienced in the lithosphere remains essentially the same. Similar insensitivity to displacement is also found for the stress exponent; when solving Eq. (2) for shear stress in upper mantle, we are actually solving for  $\sigma^n$  in the flow laws, so the effects of uncertainty in the stress exponent are not visible in predicted displacements.

In summary, with flow law parameters varying in their likely uncertainty ranges, predicted displacements between surface and 200 km depth all lie in a geologically acceptable range. Large activation energy and small activation volume favor small displacement, while the other parameter uncertainties have little influence on it.

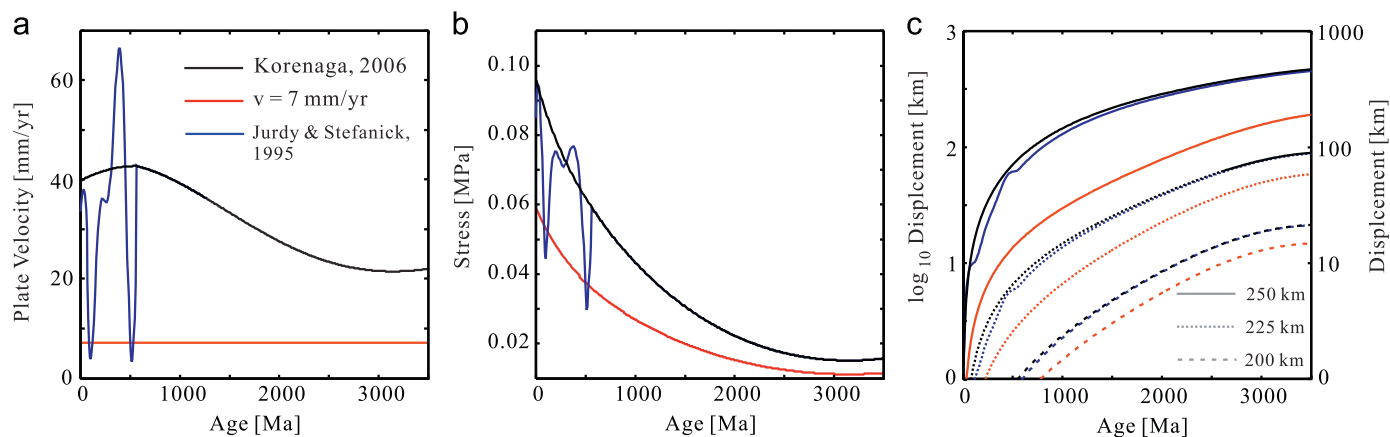


**Fig. 6.** Modeling results with more realistic plate velocities. (a) Assumed history of plate velocity; constant at 7 mm/yr (red), prediction by thermal evolution modeling by Korenaga (2006) (black), and with Phanerozoic plate velocity reconstruction by Jurdy et al. (1995) (blue). Stress evolution and displacement corresponding to each model velocity are shown in (b) and (c). (For interpretation of the references to color in this figure legend, the reader is referred to the web version of this article.)

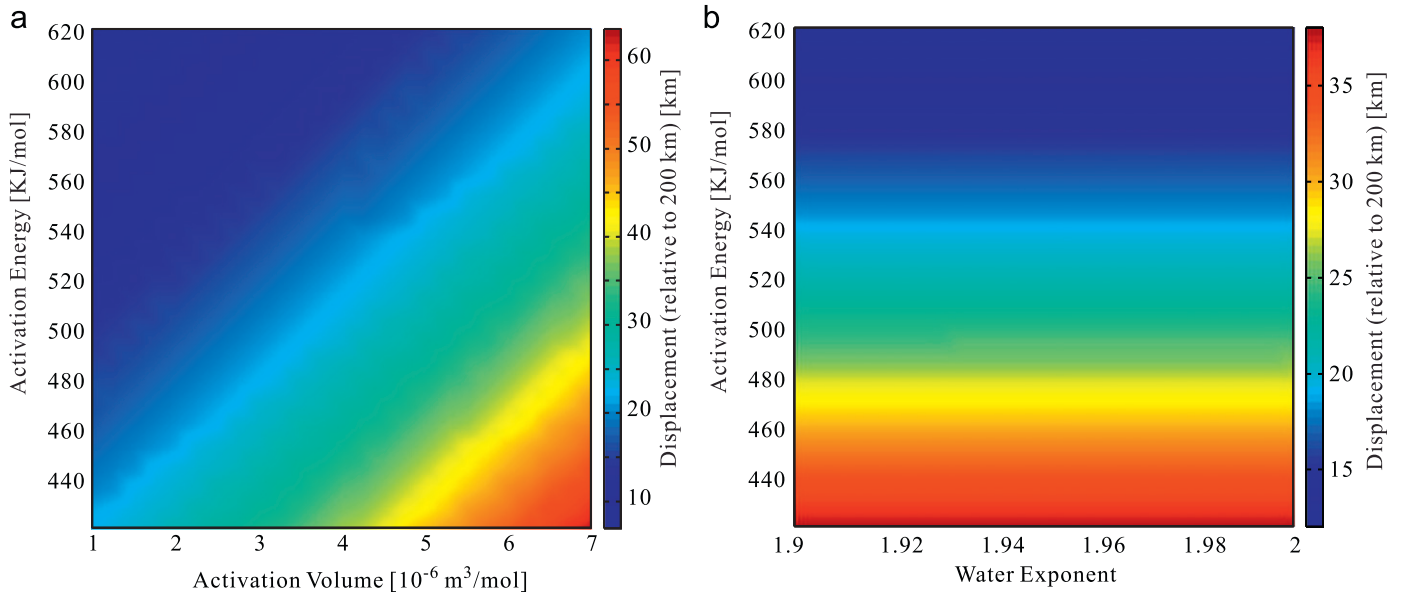


**Fig. 7.** Dependence of displacement across lithosphere (relative to 200 km depth) on olivine flow-law parameters. Displacement is calculated with a pair of flow-law parameters for wet dislocation creep varying within their likely bounds (as suggested by Korenaga and Karato (2008)) while fixing other parameters. (a) Activation energy and activation volume, and (b) activation energy and water exponent.

## 5.2. On grain-growth kinetics in the lithospheric mantle

One robust result in our modeling is the magnitude of shear stress in the upper mantle, which is considerably lower than previous estimates using grain-size-based piezometric laws that reflect dynamic recrystallization. At steady-state deformation achieved by dynamic recrystallization, grain size is related to stress empirically as (e.g. Karato et al., 1980; van der Wal et al., 1993)

$$L_g = A_g \sigma^{-r_g}, \quad (5)$$

where  $L_g$  is grain size,  $\sigma$  is stress, and  $A_g$  and  $r_g$  are constants not sensitive to temperature and pressure. Theoretical derivations (Austin and Evans, 2007; Ricard and Bercovici, 2009; Rozel et al., 2011) suggest that the grain size is conceptually a ‘paleowattmeter’ that reflects the rate of energy dissipation, rather than a ‘paleopiezometer’ that measures the deviatoric stress, but the empirical constitutive relation in Eq. (5) is still useful, with parameters either derived from deformation experiments (e.g. Jung and Karato, 2001; van der Wal et al., 1993) or estimated from natural rocks in ductile shear zones (e.g., Goetze, 1975; Nicolas, 1978). This relation provides a useful tool to estimate paleostresses from the microstructure of naturally deformed rocks in mylonite zones (e.g. White, 1979). Strain rates in deformation experiments ( $10^{-5} \text{ s}^{-1}$ ) and ductile shearing zones ( $10^{-12}$ – $10^{-14} \text{ s}^{-1}$ ) are, however, both much higher than those in the stable continental lithosphere ( $10^{-16}$ – $10^{-17} \text{ s}^{-1}$ ), and a simple application of Eq. (5) to cratonic xenoliths may not be warranted (though these xenoliths were likely to have experienced dislocation creep according to our results in Section 4). As discussed above, our estimate on stress in the continental lithosphere is about two orders of magnitude lower than that estimated with grain-size-based piezometers (e.g. Ave Lallement et al., 1980). By the same token, if we apply Eq. (5) to derive equilibrium grain size from our stress estimate, we would predict too large grain size to be consistent with xenolith observations (Fig. 8).

Previous studies based on the dislocation density of olivine grains all suggest stresses even higher than those piezometric estimates. Some of these studies are summarized in Skemer and Karato (2008), and a recent study by Arndt et al. (2010) gives the

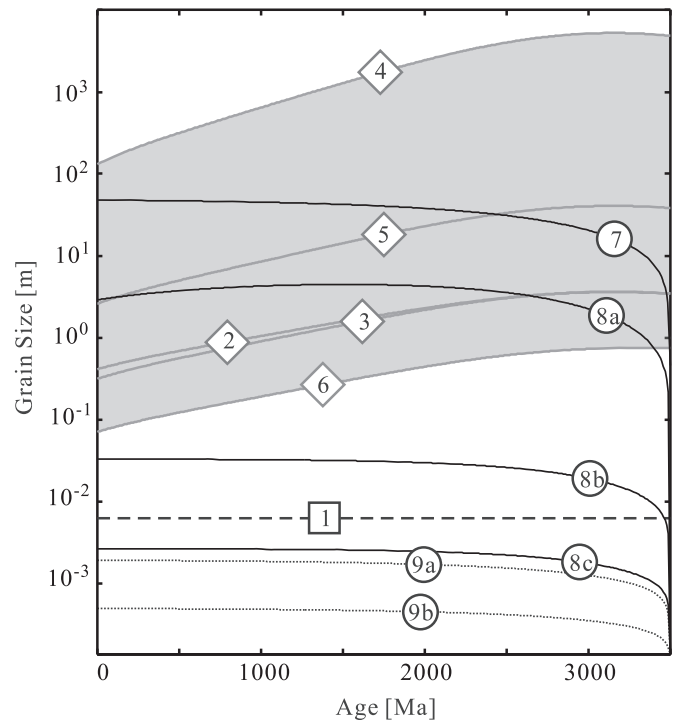


**Fig. 8.** Grain size evolution in lithosphere at depth 200 km. Dashed curve 1 denotes constant grain size of 7 mm, average of grain sizes observed in mantle xenoliths (Ave Lallement et al., 1980). Gray curves in shaded area denote grain size prediction according to dynamic recrystallization, using stress calculated in this study (Fig. 6b, black curve); 2.  $L_g = 10^{4.41} \sigma^{-1.18}$  ( $L_g$  in mm,  $\sigma$  in MPa; Jung and Karato, 2001); 3.  $L_g = 10^{4.14} \sigma^{-1.33}$  ( $L_g$  in mm,  $\sigma$  in MPa; van der Wal, 1993); 4.  $\sigma = 11 L_g^{-0.5}$  ( $L_g$  in  $\mu\text{m}$ ,  $\sigma$  in kbar; Goetze, 1975); 5.  $\sigma = 19 L_g^{-0.67}$  ( $L_g$  in  $\mu\text{m}$ ,  $\sigma$  in kbar; Post, 1973); and 6. Temperature-dependent law,  $L_g = 1.13 \sigma^{-1.4} \exp(13500/RT)$  ( $L_g$  in  $\mu\text{m}$ ,  $\sigma$  in kbar; Mercier, 1976). Solid curve 7 denotes grain-size evolution according to the monomineralic grain-growth law (see text for details), starting with  $L_0 = 0.1 \text{ mm}$  at 3.5 Ga,  $n = 2$ ,  $H = 160 \text{ kJ/mol}$ , and  $k_0 = 10^{4.2} \mu\text{m}^2 \text{ s}^{-1}$  (Karato, 1989); Solid curves 8a, b and c denote grain-size evolution predicted with the thermodynamically self-consistent damage equation (Rozel et al., 2011) with growth exponent  $p = 2, 3$ , and 4, respectively; Dotted curves 9a and b denote grain-size evolution calculated with the grain-growth parameters suggested by Hiraga et al. (2010),  $f_{EN} = 0.2$ , and growth exponent (a)  $p = 4$  and (b)  $p = 5$ .

estimate of stress in a range of 100–400 MPa. Such high stress level, however, corresponds to extremely high strain rate, and these authors suggest that it is unlikely to be related to continental drift or sublithospheric convection. Skemer and Karato (2008), for example, speculated that their samples might have been sheared by a rapidly rising plume, whereas Arndt et al. (2010) conjectured that the inferred high stress might originate in a transient phenomenon associated with the formation of kimberlite magma. Also note that the type of lattice-preferred orientation varies as a function of stress and water content, but cratonic xenoliths commonly exhibit A-type fabric, and as Katayama and Korenaga (2011) argued, this fabric information may be used to place an upper limit on the water content, but it is not useful as stress indicator because A-type fabric has no lower bound for stress. Thus, it remains unclear how these microstructures can constrain the stress level associated with continental drift, which is our main focus in this study.

A simple order-of-magnitude calculation suggests that our stress estimate should not be seen as a surprising result. Shear strain rate is of the order of  $10^{-15} \text{ s}^{-1}$  (i.e., typical geological strain rate) for a surface velocity of 10 mm/yr with a non-slip boundary at 410-km depth, and corresponding shear stress can be derived by multiplying asthenospheric viscosity with the strain rate, e.g., 0.01 MPa for the viscosity of  $10^{19} \text{ Pa s}$ , or 0.1 MPa for  $10^{20} \text{ Pa s}$ . The discrepancy between our stress estimate and that based on grain-size piezometers thus warrants careful consideration.

One possible explanation for this discrepancy is that the typical grain size of mantle xenoliths (5–10 mm) reflects a high stress level experienced during the formation of the craton in the early Archean, and olivine grains in the lithospheric mantle could not grow fast enough to reach a dynamic equilibrium with the subsequent low stress level. This idea may be tested using grain-growth kinetics, which is generally expressed as (Hillert, 1965):

$$L^p - L_0^p = k_p t, \quad (6)$$

where  $L$  is grain size,  $L_0$  is initial grain size,  $n$  is the grain-size exponent,  $t$  is time and  $k_n$  is a temperature-dependent parameter:

$$k_p = k_0 \exp(-E/RT), \quad (7)$$

where  $E$  is activation energy and  $k_0$  is a pre-exponential constant. We calculate grain-growth evolution in the lithosphere at the

depth of 200 km for the last 3.5 Gyr, starting with grain size 0.1 mm, using parameters determined for pure olivine aggregates (Karato, 1989). The initial grain size of 0.1 mm is close to the lower limit of grain size during the early stage of crystallization in a putative magma ocean (Solomatov, 2000, 2007). The grain-growth curve soars dramatically during the first few million years and gradually reaches a quasi-steady-state size of  $> 10 \text{ m}$  (curve 7 in Fig. 8). Thus, it may appear that olivine grains can grow sufficiently quickly to the size predicted by dynamic recrystallization.

One cannot, however, simply apply grain-growth kinetics derived from monomineralic aggregates to polyminerale rocks. For example, secondary phase particles are known to have a significant influence on grain-boundary migration. If a minor phase is 'indigestible' in olivine, such as orthopyroxene (opx), moving boundaries have to increase their area in order to pass these 'pinning' particles. Excess energy is thus required for increased surface energy, which slows down boundary migration and grain growth (Karato, 2008). The influence of opx pinning is estimated by Evans et al. (2001) for olivine grain growth based on data for grain-boundary mobility, assuming that grain growth is controlled by Si diffusion on grain boundaries. With opx pinning, the 'steady state' grain size is estimated to be around 10 mm, close to typical grain sizes observed in natural xenoliths. In the study of Evans et al. (2001), however, the grain size of mantle xenoliths was also thought to be consistent with dynamic recrystallization, based on the notion of high lithospheric stress, so the origin of the observed grain size remains equivocal. With the very low shear stress ( $< 0.1 \text{ MPa}$ ) estimated in this study, therefore, the grain size of cratonic olivine forms a unique observational support for the opx pinning mechanism.

In general, grain-growth kinetics is not well understood in realistically complicated systems owing to a number of controlling factors. Observed grain sizes in the lithospheric mantle could thus provide a useful (albeit crude) constraint on some sort of 'effective' grain-growth kinetics. We calculate the present grain size at 200 km depth with the same starting condition (0.1 mm at 3.5 Ga) but different grain-growth parameters ( $E$ ,  $k_0$ , and  $n$ ), and results suggest that large activation energy, small pre-exponential factor  $k_0$ , and small grain-growth exponent favor small grain size (Fig. 9), which is largely intuitive. We tested two possible growth

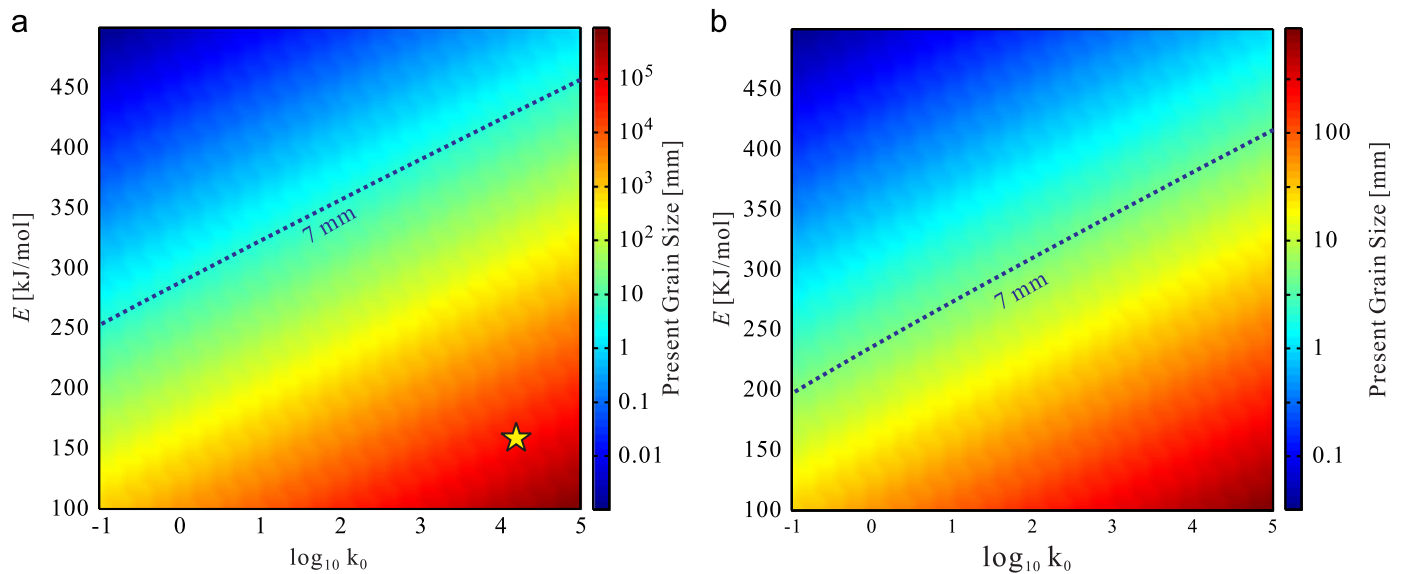


**Fig. 9.** Calculated present-day grain size (at 200 km depth) and its dependence on grain-growth parameters (activation energy  $E$ , pre-exponential factor  $k_0$  and grain size exponent  $p$ ). Observed grain size (7 mm, Ave Lallement et al., 1980) is shown as dotted line. Yellow star represents the grain-growth law for pure olivine aggregates (Karato, 1989). (For interpretation of the references to color in this figure legend, the reader is referred to the web version of this article.) (a)  $p=2$  and (b)  $p=4$ .

exponents,  $p=2$  and 4; the former is applicable for pure olivine aggregates (Karato, 1989), and the latter is based on the work of Faul and Scott (2006) and Ohuchi and Nakamura (2007) on opx-rich peridotites, in which the presence of pyroxene inhibits the grain growth of olivine. With the pre-exponential factor and the growth exponent being the same as those for pure olivine aggregates, the activation energy should be higher than  $\sim 400$  kJ/mol to explain the observed small grain size. Or, if we choose to keep the activation energy at  $\sim 150$  kJ/mol instead, the pre-exponential factor needs to be lowered by about ten orders of magnitude.

We have also considered more recent studies on grain size evolution. First, Hiraga et al. (2010) experimentally investigated grain growth kinetics of olivine and opx as a function of volume fraction of opx ( $f_{En}$ ). Their experiments were done at  $T=1360 \pm 5$  °C, which is close to the temperature at 200 km depth in our model. Predicted grain growth curves at 200 km depth, based on their suggested grain growth law, are shown in Fig. 8, using  $f_{En}=0.2$  (average opx fraction for cratonic xenoliths; Pearson et al., 2003) and the growth exponents of  $p=4$  (Curve 9a) and  $p=5$  (Curve 9b). The predicted grain size with the growth exponent of  $p=4$  is of millimeter scale, whereas that with  $p=5$  is too small to be realistic. Fig. 9b suggests that with  $p=4$  and with the same activation energy for monomineralic olivine grain growth, the pre-exponential factor needs to be lower than  $10^{-2}$ , close to the value suggested in Hiraga et al. (2010). Second, Ricard and Bercovici (2009) and Rozel et al. (2011) derived a thermodynamically self-consistent damage equation for grain-size evolution that involves both grain growth and recrystallization. In their formalism, the grain size reduction term is controlled by mechanical dissipation and can be calculated with our estimate on stress evolution. Dislocation creep is the dominant mechanism of deformation, so we neglect the contribution of varying grain-size to the dissipation term. Predicted grain-size evolutions are shown in Fig. 8 with the growth exponents of  $p=2$  (Curve 8a), 3 (Curve 8b), and 4 (Curve 8c). The grain-growth parameters are adopted from Kameyama et al. (1997) and flow-law parameters from Korenaga and Karato (2008). The grain-size evolution with  $p=4$  is very close to the calculation using the results of Hiraga et al. (2010), which is understandable because a higher growth exponent corresponds to a greater effect of secondary phase pinning.

In summary, simple grain-size-based piezometers are not applicable to cratonic xenoliths. Grain growth laws derived in monomineralic systems should be used with caution in natural rocks, because other factors, like secondary phase pinning, can significantly slow down the rate of grain growth. With growth exponent  $p=4$  and a corresponding empirical pre-exponential value suggested in Hiraga et al. (2010), the predicted grain size is of similar magnitude as observed in xenoliths. Our observational bounds on the permissible range of effective grain growth parameters (Fig. 9) are shown to be in a good agreement with the experimental study of Hiraga et al. (2010) and the theoretical study of Rozel et al. (2011).

## 6. Conclusions

We have shown how to convert qualitative observations on geochronological patterns exhibited by cratonic xenoliths into quantitative constraints on the magnitude of shear stress associated with continental drift as well as effective grain-growth kinetics in the lithospheric mantle. In doing so, we were also able to test the flow-law parameters for olivine rheology. The parameters recommended by Korenaga and Karato (2008) are shown to be consistent with relatively small lithospheric-scale deformation

indicated by cratonic xenoliths. Varying these parameters within their estimated uncertainties hardly affect this geological consistency, meaning that this study by itself does not help to reduce the parameter uncertainty.

Our results suggest that stress in the lithosphere increased from  $\sim 0.01$  MPa to  $\sim 0.1$  MPa in the past 3.5 billion years, which is about two orders of magnitude lower than previous estimates based on grain-size piezometers. With the grain-growth kinetics of pure olivine aggregates, olivine grains must have grown to the size of  $\sim 1$  m, as opposed to the observed range of 5–10 mm. We interpret this discrepancy as observational support for retarded grain growth by orthopyroxene pinning. In order to capture the effect of pinning by an 'effective' grain-growth law, the growth exponent  $p=4$  is a likely estimate. This constraint on grain growth in the lithospheric mantle over the last 3.5 Gyr is based on the observed grain size in kimberlite xenolith, so despite its crude nature, it will be a useful constraint when discussing long-term mantle dynamics.

## Appendix A. Supporting information

Supplementary data associated with this article can be found in the online version at <http://dx.doi.org/10.1016/j.epsl.2012.04.019>.

## References

- Arndt, N.T., Guitreau, M., Boullier, A.-M., Le Roex, A., Tommasi, A., Cordier, P., Sobolev, A., 2010. Olivine, and the origin of kimberlite. *J. Petrol.* 51, 573–602.
- Austin, N.J., Evans, B., 2007. Paleowattmeters: a scaling relation for dynamically recrystallized grain size. *Geology* 35, 343–346.
- Ave Lallement, H.G., Mercier, J.-C.C., Carter, N.L., Ross, J.V., 1980. Rheology of the upper mantle: inferences from peridotite xenoliths. *Tectonophysics* 70, 85–113.
- Bell, D.R., Rossman, G.R., 1992. Water in Earth's mantle: the role of nominally anhydrous minerals. *Science* 255, 1391–1397.
- Boyd, F.R., Nixon, P.H., 1975. Origins of the ultramafic nodules from some kimberlites of northern Lesotho and the Monastery mine, South Africa. *Phys. Chem. Earth* 9, 431–454.
- Bradley, D.C., 2008. Passive margins through earth history. *Earth-Sci. Rev.* 91, 1–26.
- Bürgmann, R., Dresen, G., 2008. Rheology of the lower crust and upper mantle: evidence from rock mechanics, geodesy and field observations. *Annu. Rev. Earth Planet. Sci.* 36, 531–567.
- Chapman, D.S., Furlong, K.P., 1992. Thermal state of the continental lower crust. In: Fountain, D.M., Arculus, R., Kay, R.W. (Eds.), *Continental Lower Crust*. Elsevier, pp. 179–199.
- Danchin, R.V., 1979. Mineral and bulk chemistry of garnet lherzolite and garnet harzburgite xenoliths from the Premier mine, South Africa. In: Boyd, F.R., Mayer, H.O.A. (Eds.), *The Mantle Sample: Inclusions in Kimberlites and Other Volcanics*. AGU, pp. 104–126.
- de Wit, M.J., Roering, C., Hart, R.J., Armstrong, R.A., de Ronde, C.E.J., Green, R.W.E., Tredoux, M., Peberdy, E., Hart, R.A., 1992. Formation of an Archean continent. *Nature* 357, 553–562.
- Dijkstra, A.H., Drury, M.R., Vissers, R.L.M., Newman, J., Van Roermund, H.L.M., 2004. Shear zones in the upper mantle: evidence from alpine- and ophiolite-type peridotite massifs. *Geol. Soc. London Spec. Publ.* 224, 11–24.
- Eaton, D.W., Darbyshire, F., Evans, R.L., Grütter, H., Jones, A.G., Yuan, X., 2009. The elusive lithosphere–asthenosphere boundary (LAB) beneath cratons. *Lithos* 109, 1–22.
- Evans, B., Renner, J., Hirth, G., 2001. A few remarks on the kinetics of static grain growth in rock. *Int. J. Earth Sci.* 90, 88–103.
- Evans, R.L., Jones, A.G., Xavier, G., Muller, M., Hamilton, M., Evans, S., Fourie, C.J.S., Spratt, J., Webb, S., Jelsma, H., Hutchines, D., 2011. Electrical lithosphere beneath the Kaapvaal craton, southern Africa. *J. Geophys. Res.* 116, B04105 <http://dx.doi.org/10.1029/2010JB007883>.
- Faul, U.H., Scott, D., 2006. Grain growth in partially molten olivine aggregates. *Contrib. Mineral. Petrol.* 151, 101–111.
- Goetze, C., 1975. Sheared lherzolites: from the point of view of rock mechanics. *Geology* 3, 172–173.
- Griffin, W.L., O'Reilly, S.Y., Natapov, L.M., Ryan, C.G., 2003. The evolution of lithospheric mantle beneath the Kalahari Craton and its margins. *Lithos* 71, 215–241.
- Gripp, A.E., Gordon, R.G., 2002. Young tracks of hotspots and current plate velocities. *J. Int.* 150, 321–361.

- Gueguen, Y., Nicolas, A., 1980. Deformation of mantle rocks. *Annu. Rev. Earth Planet. Sci.* 8, 119–144.
- Herzberg, C., Condie, K., Korenaga, J., 2010. Thermal history of the Earth and its petrological expression. *Earth Planet. Sci. Lett.* 292, 79–88.
- Hillert, M., 1965. On the theory of normal and abnormal grain growth. *Acta Metall.* 13, 227–238.
- Hiraga, T., Tachibana, C., Ohashi, N., Sano, S., 2010. Grain growth systematics for forsterite ± enstatite aggregates: effect of lithology on grain size in the upper mantle. *Earth Planet. Sci. Lett.* 291, 10–20.
- Hirth, G., Kohlstedt, D.L., 1996. Water in the oceanic mantle: implications for rheology, melt extraction, and the evolution of the lithosphere. *Earth Planet. Sci. Lett.* 144, 93–108.
- Hirth, G., Kohlstedt, D.L., 2003. Rheology of the upper mantle and the mantle wedge: a view from the experimentalists. In: Eiler, J. (Ed.), *Inside the Subduction Factory*. AGU, Washington, D.C., pp. 83–105.
- Hoffman, P.F., 1997. Tectonic genealogy of North America. In: van der Pluijm, B.A., Marshak, S. (Eds.), *Earth Structure: An Introduction to Structural Geology and Tectonics*. McGraw-Hill, New York, pp. 459–464.
- Hofmeister, A., 1999. Mantle values of thermal conductivity and the geotherm from phonon lifetimes. *Science* 283, 1699–1709.
- Holland, T.J.B., Powell, R., 1998. An internally consistent thermodynamic data set for phases of petrological interest. *J. Metamorphic Geol.* 16, 309–343.
- James, D.E., Fouch, M.J., Van Decar, J.C., van der Lee, S., 2001. Tectospheric structure beneath Southern Africa. *Geophys. Res. Lett.* 28, 2485–2488.
- Jaupart, C., Mareschal, J.C., 1999. The thermal structure and thickness of continental roots. *Lithos* 24, 93–114.
- Jin, D., Karato, S.-I., Obata, M., 1998. Mechanisms of shear localization in the continental lithosphere: inference from the deformation microstructures of peridotites from the Ivrea zone, northwestern Italy. *J. Struct. Geol.* 20, 195–209.
- Jones, M.Q.W., 1988. Heat flow in the Witwatersrand Basin and environs and its significance for the South African Shield geotherm and lithosphere thickness. *J. Geophys. Res.* 93, 3243–3260.
- Jung, H., Karato, S.-I., 2001. Effects of water on dynamically recrystallized grain-size of olivine. *J. Struct. Geol.* 23, 1337–1344.
- Jurdy, D.M., Stefanick, M., Scotese, C.R., 1995. Paleozoic plate dynamics. *J. Geophys. Res.* 100, 17,965–17,975.
- Karato, S., Toriumi, M., Fujii, T., 1980. Dynamic recrystallization of olivine single crystals during high temperature creep. *Geophys. Res. Lett.* 7, 649–652.
- Karato, S., 1989. Grain growth kinetics in olivine aggregates. *Tectonophysics* 168, 255–273.
- Karato, S., 2008. *Deformation of Earth Materials: An Introduction to the Rheology of Solid Earth*. Cambridge University Press, Cambridge.
- Kameyama, M., Yuen, D.A., Fujimoto, H., 1997. The interaction of viscous heating with grain-size dependent rheology in the formation of localized slip zones. *Geophys. Res. Lett.* 24, 2523–2526.
- Katayama, I., Korenaga, J., 2011. Is the African cratonic lithosphere wet or dry? In: Beccaluva, L., Bianchini, G., Wilson, M. (Eds.), *Volcanism and Evolution of the African Lithosphere*, 478. GSA, pp. 249–256. (special papers).
- Korenaga, J., 2006. Archean geodynamics and the thermal evolution of Earth. In: Benn, K., Mareschal, J.-C., Condie, K. (Eds.), *Archean Geodynamics and Environments*. AGU, pp. 7–32.
- Korenaga, J., 2008. Urey ratio and the structure and evolution of Earth's mantle. *Rev. Geophys.* 46, RG2007, <http://dx.doi.org/10.1029/2007RG000241>.
- Korenaga, J., Karato, S.-I., 2008. A new analysis of experimental data on olivine rheology. *J. Geophys. Res.* 113, B02403, <http://dx.doi.org/10.1029/2007JB005100>.
- Korenaga, J., Jordan, T.H., 2002. On the state of sublithospheric upper mantle beneath a supercontinent. *Geophys. J. Int.* 149, 179–189.
- Kurosawa, M., Yurimoto, H., Sueno, S., 1997. Patterns in the hydrogen and trace element compositions of mantle olivines. *Phys. Chem. Miner.* 24, 385–395.
- Lazarov, M., Woodland, A.B., Brey, G.P., 2009. Thermal state and redox conditions of Kaapvaal mantle: a study of xenoliths from the Finsch mine, South Africa. *Lithos* 112 (Suppl. 2), 913–923.
- McKenzie, D., Jackson, J., Priestley, K., 2005. Thermal structure of oceanic and continental lithosphere. *Earth Planet. Sci. Lett.* 233, 337–349.
- Mei, S., Kohlstedt, D.L., 2000a. Influence of water on plastic deformation of olivine aggregates. 1. Diffusion creep regime. *J. Geophys. Res.* 105, 21,457–21,469.
- Mei, S., Kohlstedt, D.L., 2000b. Influence of water on plastic deformation of olivine aggregates. 2. Dislocation creep regime. *J. Geophys. Res.* 105, 21,471–21,481.
- Mercier, J.C., 1976. *Natural Peridotites: Chemical and Rheological Heterogeneity of the Upper Mantle*. Ph.D. Thesis. Earth and Planetary Science Department, University of New York, Stony Brook.
- Michaut, C., Jaupart, C., Bell, D.R., 2007. Transient geotherms in Archean continental lithosphere: new constraints on thickness and heat production of subcontinental lithospheric mantle. *J. Geophys. Res.*, 112.
- Miller, G.H., Rossman, G.R., Harlow, G.E., 1987. The natural occurrence of hydroxide in olivine. *Phys. Chem. Miner.* 14, 461–472.
- Nguuri, T.K., Gore, J., James, D.E., Webb, S.J., Wright, C., Zengeni, T.G., Gwavava, O., Snoke, J.A., 2001. Crustal structure beneath southern Africa and its implications for the formation and evolution of the Kaapvaal and Zimbabwe cratons. *Geophys. Res. Lett.* 28, 2501–2504.
- Nicolas, A., 1978. Stress estimates from structural studies in some mantle peridotites. *Philos. Trans. R. Soc. London A* 288, 49–57.
- Nicolaysen, L.O., Hart, R.J., Gale, N.H., 1981. The Vredefort radioelement profile extended to supracrustal strata at Carletonville, with implications for continental heat flow. *J. Geophys. Res.* 86, <http://dx.doi.org/10.1029/JB086iB11p10653>.
- Niu, F., James, D.E., 2002. Fine structure of the lowermost crust beneath the Kaapvaal craton and its implications for crustal formation and evolution. *Earth Planet. Sci. Lett.* 200, 121–130.
- Ohuchi, T., Nakamura, M., 2007. Grain growth in the forsterite–diopside system. *Phys. Earth Planet. Inter.* 160, 1–21.
- Pearson, D.G., Carlson, R.W., Shirey, S.B., Boyd, F.R., Nixon, P.H., 1995. The stabilization of Archean lithospheric mantle: a Re–Os isotope study of peridotite xenoliths from the Kaapvaal craton. *Earth Planet. Sci. Lett.* 134, 341–357.
- Pearson, D.G., 1999. The age of continental roots. *Lithos* 48, 171–194.
- Pearson, D.G., Canil, D., Shirey, S.B., 2003. Mantle samples included in volcanic rocks: xenoliths and diamonds. In: Carlson, R.W. (Ed.), *Treatise on Geochemistry*, vol. 2. Elsevier, pp. 171–277.
- Peslier, A.H., Luhr, J.F., 2006. Hydrogen loss from olivines in mantle xenoliths from Simcoe (USA) and Mexico: mafic alkalic magma ascent rates and water budget of sub-continental lithosphere. *Earth Planet. Sci. Lett.* 242, 302–319.
- Peslier, A.H., Woodland, A.B., Bell, D.R., Lazarov, M., 2010. Olivine water contents in continental lithosphere and the longevity of cratons. *Nature* 467, 78–81.
- Post, R., 1973. *The Flow Laws of Mt. Burnett Dunite*. Ph.D. Thesis. Geophysics Department, University of California, Los Angeles.
- Press, W.H., Teukolsky, S.A., Vetterling, W.T., Flannery, B.P., 1992. *Numerical Recipes in C*, 2nd ed. Cambridge University Press.
- Ricard, Y., Bercovici, D., 2009. A continuum theory of grain size evolution and damage. *J. Geophys. Res.* 114, B011204, <http://dx.doi.org/10.1029/2007JB005491>.
- Rozel, A., Ricard, Y., Bercovici, D., 2011. A thermodynamically self-consistent damage equation for grain size evolution during dynamic recrystallization. *Geophys. J. Int.* 184, 719–728.
- Schmitz, M.D., Bowring, S.A., de Wit, M.J., Gartz, V., 2004. Subduction and terrane collision stabilize western Kaapvaal craton tectosphere 2.9 billion years ago. *Earth Planet. Sci. Lett.* 222, 363–376.
- Skemer, P., Karato, S.-I., 2008. Sheared lherzolite xenoliths revisited. *J. Geophys. Res.* 113, B07205, <http://dx.doi.org/10.1029/2007JB005286>.
- Solomatov, V.S., 2000. Fluid dynamics of a terrestrial magma ocean. In: Canup, R., Righter, K. (Eds.), *Origin of the Earth and Moon*. University of Arizona Press, Tucson, Arizona, pp. 323–338.
- Solomatov, V.S., 2007. Magma oceans and primordial mantle differentiation. In: Schubert, G. (Ed.), *Treatise on Geophysics*, vol. 9. Elsevier, pp. 91–120.
- Stankiewicz, J., Chevrot, S., van der Hilst, R.D., de Wit, M.J., 2002. Crustal thickness, discontinuity depth, and upper mantle structure beneath southern Africa: constraints from body wave conversions. *Phys. Earth Planet. Inter.* 130, 235–251.
- Taylor, S.R., McLennan, S.M., Armstrong, R.L., Tarney, J., 1981. The composition and evolution of the continental crust: rare earth element evidence from sedimentary rocks. *Philos. Trans. R. Soc. A* 301, 381–399.
- Turcotte, D.L., Schubert, G., 2002. *Geodynamics*, 2nd ed. Cambridge Univ. Press, Cambridge.
- van der Wal, D., Chopra, P.N., Drury, M., Fitz Gerald, J.D., 1993. Relationships between dynamically recrystallized grain size and deformation conditions in experimentally deformed olivine rocks. *Geophys. Res. Lett.* 20, 1479–1482.
- Vissers, R.L.M., Drury, M.R., Strating, E.H.H., Spiers, C.J., van der Wal, D., 1995. Mantle shear zones and their effect on lithosphere strength during continental breakup. *Tectonophysics* 249, 155–171.
- White, S.H., 1979. Grain and sub-grain size variations across a mylonite zone. *Contrib. Mineral. Petrol.* 70, 193–202.
- Whittington, A.G., Hofmeister, A.M., Nabelek, P.I., 2009. Temperature-dependent thermal diffusivity of Earth's crust and implications for magmatism. *Nature* 458, 319–321.